Non-coding RNA Research 9 (2024) 1190–1202

Contents lists available at ScienceDirect

Non-coding RNA Research

journal homepage: www.keaipublishing.com/en/journals/non-coding-rna-research

Original Research Article

The role of exosomal lncRNAs in acetaminophen-induced induced liver injury in SD rats

Zixuan Yang [a,b,1], Lei Shi [a,b,1], Minhui Zheng [a,b], Minbo Hou [b], Mengdi Zhou [b], Naying Su [b], Hui Lang [b], Liyuan Zhao [c,d], Mengyun Gu [a,b], Naping Tang [a,b,d,**], Yan Chang [a,b,*]

[a] China State Institute of Pharmaceutical Industry, Shanghai, 201203, China
[b] Shanghai Innostar Bio-Technology Co., Ltd, Shanghai, 201203, China
[c] College of Pharmacy, Anhui University of Chinese Medicine, Hefei, Anhui, 230000, China
[d] Yangtze Delta Drug Advanced Research Institute, Yangtze Delta Pharmaceutical College, Nantong, Jiangsu, 226133, China

ARTICLE INFO

Keywords:
Exosome
LncRNA
RNA sequencing
PCR
DILI

ABSTRACT

Background: Drug-induced liver injury (DILI) is a leading cause of drug development failures during clinical trials and post-market introduction. Current biomarkers, such as ALT and AST, lack the necessary specificity and sensitivity needed for accurate detection. Exosomes, which protect LncRNAs from RNase degradation, could provide reliable and easily accessible options for biomarkers.

Materials and methods: RNA-sequencing was used to identify differentially expressed LncRNAs (DE-LncRNAs), followed by isolation of LncRNAs from plasma exosomes in this study. Exosome characterization was conducted by transmission electron microscopy (TEM), nanoparticle tracking analysis (NTA), and Western blot (WB). Bioinformatics analysis included functional enrichment and co-expression network analysis. Five rat models were established, and quantitative real-time PCR was used to verify the specificity and sensitivity of two candidate exosomal LncRNAs.

Results: The APAP-induced hepatocellular injury model was successfully established for RNA-sequencing, leading to the identification of several differentially expressed exosomal LncRNAs. Eight upregulated exosomal DE-LncRNAs were selected for validation. Among them, NONRATT018001.2 ($p < 0.05$) and MSTRG.73954.4 ($p < 0.05$) exhibited a more than 2-fold increase in expression levels. In hepatocellular injury and intrahepatic cholestasis models, both NONRATT018001.2 and MSTRG.73954.4 showed earlier increases compared to serum biomarkers ALT and AST. However, no histological changes were observed until the final time point. In the fatty liver model, NONRATT018001.2 and MSTRG.73954.4 increased earlier than ALT and AST at 21 days. By the 7th day, minor steatosis was evident in liver tissue, while the expression levels of the two candidate exosomal LncRNAs exceeded 2 and 4 times, respectively. In the hepatic fibrosis model, NONRATT018001.2 and MSTRG.73954.4 showed increases at every time point. By the 49th day, hepatocellular necrosis and fibrosis were observed in the liver tissue, with NONRATT018001.2 showing an increase of more than 8 times. The specificity of the identified exosomal DE-LncRNAs was verified using a myocardial injury model and they showed no significant differences between the case and control groups.

Conclusion: NONRATT018001.2 and MSTRG.73954.4 hold potential as biomarkers for distinguishing different types of organ injury induced by drugs, particularly enabling early prediction of liver injury. Further experiments, such as siRNA interference or gene knockout, are warranted to explore the underlying mechanisms of these LncRNAs.

* Corresponding author. China State Institute of Pharmaceutical Industry, Shanghai Innostar Bio-Technology Co., Ltd., 199 Guoshoujing Road, Pilot FreeTrade Zone, Shanghai, 201203, China.
** Corresponding author. China State Institute of Pharmaceutical Industry, Shanghai Innostar Bio-Technology Co., Ltd., 199 Guoshoujing Road, Pilot FreeTrade Zone, Shanghai, 201203, China.
E-mail addresses: 18116277430@163.com (Z. Yang), lshi@innostar.cn (L. Shi), zmh15552737550@163.com (M. Zheng), mbhou@innostar.cn (M. Hou), mdzhou@innostar.cn (M. Zhou), nysu@innosar.cn (N. Su), hlang@innostar.cn (H. Lang), zly541186@163.com (L. Zhao), mygu@innostar.cn (M. Gu), napingtang@innostar.cn (N. Tang), ychang@innostar.cn (Y. Chang).
[1] These authors contributed equally to this work and should be considered co-first authors.

https://doi.org/10.1016/j.ncrna.2024.05.011
Received 27 March 2024; Received in revised form 12 May 2024; Accepted 21 May 2024
Available online 23 May 2024

1. Introduction

Drug-induced liver injury (DILI) is a potentially life-threatening adverse event triggered by drugs and other compounds. Although complex in its origins, DILI is relatively rare in clinical settings, yet presents significant challenges in terms of prediction, diagnosis, and management [1–4]. Idiosyncratic DILI (iDILI) accounts for 23 % of hospitalizations due to adverse drug reactions [5], and contributes to 11 % of cases of acute liver failure (ALF) in developed countries. Notably, acetaminophen (paracetamol, APAP) overdose, a prime example of intrinsic, predictable DILI, is responsible for 50 % of all ALF cases attributed to drug toxicity [6]. Thus, DILI poses serious risks to patients' safety and is a significant concern for regulatory authorities. DILI represents a major factor in drug withdrawals from the market due to its frequent occurrence during clinical development.

DILI can be classified into two types: idiosyncratic and intrinsic hepatotoxicity. Intrinsic DILI refers to drugs that can cause liver injury in animal models and humans when administered at sufficiently high doses. Conversely, idiosyncratic DILI is rare, affecting only susceptible individuals, and is not necessarily dependent on dosage [7]. DILI encompasses a wide range of histological and clinical manifestations, including acute steatosis, cholestasis, and hepatocellular damage, often detected in late stages of phase III clinical trials or during post-marketing surveillance.

APAP hepatotoxicity serves as the paradigmatic model for DILI and holds particular relevance to human DILI due to the widespread consumption of analgesic doses annually. In humans, APAP hepatotoxicity can be replicated in rodents through acute or cumulative overdose, typically occurring after fasting. Rodents, particularly rats, are commonly utilized in preclinical safety assessments and toxicity investigations. For instance, previous research has demonstrated the clinical relevance of the rat model in APAP-induced hepatotoxicity [8]. In disease studies, RNA-seq technology facilitates a deeper understanding of disease pathogenesis more precisely and sheds light on the relationship between specific RNA molecules and diseases. By elucidating the precise regulation of individual genes in disease states, RNA-seq proves invaluable in identifying novel biomarkers.

Exosomes, small vesicles ranging from 30 to 150 nm in diameter, are secreted by various cells and enclosed within a lipid bilayer membrane. They are found in various bodily fluids such as peripheral blood, urine, and ascites, and consist of nucleic acids, lipids, proteins, and other molecules. These components affect disease progression through intercellular materials and information transmission, or by engaging in direct interactions with target cells [9,10]. Thus, the presence of exosomes in bodily fluids suggests their potential as a non-invasive diagnostic tool for various diseases.

While numerous studies have investigated exosomal miRNA, LncRNA, or circRNA as biomarkers for alcoholic liver diseases, viral hepatitis, cholestatic liver injury, and hepatocellular carcinoma [11], only few have focused on DILI. Therefore, we employed RNA sequencing to identify differentially expressed exosomal LncRNAs (DE-LncRNAs) and validated them through PCR. Exosome characterization was conducted via nanoparticle tracking analysis (NTA), transmission electron microscopy (TEM), and Western blot (WB) analysis. The results from several validation studies confirmed the potential of plasma exosomal DE-LncRNAs as biomarkers.

2. Materials and methods

2.1. Animals

Young adult Sprague-Dawley rats, aged 6–8 weeks and weighing between 180 and 250g, were procured from Zhejiang Vital River Laboratory Animal Technology. The animals were housed in groups under controlled conditions, with a temperature maintained between 20 and 26 °C and humidity between 40 % and 70 %. The housing facility ensured adequate ventilation, with ≥15 air exchanges per hour and 100 % fresh air supply (no air recirculation), while maintaining a 12-h light/dark cycle. Water and food were available *ad libitum*. After a 3-day quarantine period, the rats underwent screening to establish various DILI models.

The experimental protocols were conducted at Shanghai InnoStar Bio-tech Co., Ltd., an accredited animal facility adhering to the guidelines set forth by AAALAC International. The facility holds an animal use license: SYXK (Shanghai) 2019-0009. The study protocol, along with all animal care and use procedures, received approval from the Institutional Animal Care and Use Committee (IACUC) of Shanghai InnoStar Bio-Tech (IACUC number: IACUC-2022-r-147). All experiments were conducted in compliance with the institution's standard ethical guidelines.

2.2. Animal model establishment

2.2.1. Model for RNA sequencing

Hepatocellular injury model: Twenty Sprague-Dawley rats, comprising equal numbers of males and females, received a dose of 4-acetamidophenol (APAP, Aladdin, China) at 1250 mg/kg via intragastric administration (n = 10). Plasma, serum, and liver tissue samples were collected 24 h post-administration. The control group (n = 10) received 0.5 % CMC-Na and underwent sample collection 24 h after administration.

2.2.2. Models for subsequent validation

Hepatocellular injury model: Male Sprague-Dawley rats (n = 25) were administered APAP (Aladdin, China) at 1250 mg/kg via intragastric administration (10 mL/kg). Plasma, serum, and liver tissue samples were harvested from five rats at 1.5, 3, 6, 12, and 24 h post-administration for further analysis. The control rats (n = 25) were given 0.5 % CMC-Na, and samples were collected at corresponding time points for analysis.

Intrahepatic cholestasis model: Male Sprague-Dawley rats (n = 25) received 1-naphthyl isothiocyanate (ANIT, Aladdin, China) at 150 mg/kg via intragastric administration (10 mL/kg). Samples of plasma, serum, and liver tissue were collected from five rats at 1.5, 3, 6, 12, and 24 h post-administration for further analysis. The control rats (n = 25) were given corn oil (Yihai Kerry Arawana Holdings Co., Ltd, China), and samples were collected at corresponding time points for analysis.

Fatty liver model: Male Sprague-Dawley rats (n = 25) were fed a methionine choline-deficient diet (MCDD, Beijing Keao Xieli Feed Co., Ltd., China). Plasma, serum, and liver tissue samples were collected from five rats at 3 days, 1, 2, 3, and 4 weeks post-diet initiation for further analysis. The rats in control group (n = 25) received a diet containing methionine choline (with the exception of methionine choline, all other components were identical to MCDD), and samples were collected at corresponding time points for analysis.

Hepatic fibrosis model: Male Sprague-Dawley rats (n = 25) received 50 % CCl_4 (Macklin, China) via intraperitoneal injection (diluted in olive oil, 1 mL/kg), twice weekly for 8 weeks (on the first and fourth days of each week). Plasma, serum, and liver tissues were harvested from five rats at 2, 4, 6, 7, and 8 weeks for further analysis. The control group (n = 25) received olive oil (Olivoila, China) in the same manner as CCl_4, and samples were collected at corresponding time points for analysis.

Myocardial injury model: Male Sprague-Dawley rats (n = 5) received isoprenaline hydrochloride (IH, Sigma-Aldrich, China) at 2.5 mg/kg via tail intravenous injection for a single dose (10 mL/kg). Plasma, serum, and liver tissues were collected 4 h post-administration for further analysis. The control rats (n = 5) were given 0.9 % sodium chloride injection via the same administration route as IH, and specimens were collected accordingly for analysis.

Table 1
Primer sequences for qPCR.

Gene	Sequence (5′–3′)
NONRATT018001.2-F	ACCGAGGAAAGACGGAATCC
NONRATT018001.2-R	GCCTTCTATCCATCTCTGGAACA
MSTRG.46987.1-F	TTCCCTTTGACCAGCCTTGT
MSTRG.46987.1-R	GCCATTGACTCATGAGGAAGGT
MSTRG.73954.4-F	CAATCCTTCATTCCCCACTTCT
MSTRG.73954.4-R	AATGGGATGAACAATGGCTCTAA
NONRATT013926.2-F	CAAGGTGCCAGCTCGATGT
NONRATT013926.2-R	CAGAGGTGCCCCACAGGTT
NONRATT004188.2-F	TTCCCGCGTGCTCAGACT
NONRATT004188.2-R	TGAACCCAGGACCACATGAA
NONRATT008284.2-F	CAAGAGGAAAGACGTCGAATGA
NONRATT008284.2-R	TGCTGCATCAGGACGGTTTA
NONRATT023507.2-F	CTCCCACACACAGGCATCTCT
NONRATT023507.2-R	TTTCTCTTACCCCCGGTCTTG
NONRATT029616.2-F	CCTGCTGAGCTGACCTGTAGTG
NONRATT029616.2-R	CTTCTGCTTCTTGGTCTCAACATC
RAT-GAPDH-F	TGGCCTCCAAGGAGTAAGAAAC
RAT-GAPDH-R	GGCCTCTCTCTTGCTCTCAGTATC

F: forward; R: reverse.

2.3. Histology and biochemical analysis

Anesthesia was induced in Sprague-Dawley rats using a combination of Ketamine and Xylazine administered intraperitoneally (40 mg/mL Ketamine + 5 mg/mL Xylazine, 2 mL/kg). Blood specimens were obtained via the abdominal aorta.

Liver tissue was fixed in formalin, processed for conventional histology, embedded in paraffin, and sectioned (5 μm). Sections were stained with H&E according to standard protocols for histopathological assessment of liver tissues. Photomicrographs were acquired using a light microscope (Olympus, Japan).

The following parameters were assessed: Serum levels of ALT, AST, and CK were examined using a Hitachi 7060 automatic biochemical analyzer following kit instructions. Serum hsTnI levels were determined using the Access 2 immunoassay system.

2.4. Exosomes isolation and characterization

Exosomes were isolated from plasma using the exoRNeasy Midi Kit (Qiagen, Germany). Plasma was initially centrifuged (13,000×*g*, 15 min, 4 °C). The supernatant was then filtered to remove particles larger than 0.8 μm and mixed with Buffer XBP. The mixture was bound to an exoEasy spin column, washed with Buffer XWP, and then with Buffer XE.

The size distribution of exosomes was detected using the NTA instrument ZetaVIEW S/N 17–310 (Particle Metrix, Germany). Exosomes were diluted 1000-fold with buffer and analyzed. TEM (HT7700, Hitachi, Japan) was utilized to examine the morphology of exosomes. The expression of exosome marker proteins CD9, CD63, and TSG101 was assessed by WB analysis. Exosomes were lysed with RIPA buffer (Thermo Scientific), and protein specimens were separated through 10 % SDS-PAGE, transferred onto PVDF membranes, and blocked with 5 % skim milk. After washing with TBST, the membranes were exposed to primary antibodies (CD63, CD9, and TSG101 from System Biosciences, USA) overnight at 4 °C. Following washes, the membranes were exposed to secondary antibody for 1 h at room temperature. Bands were visualized using enhanced chemiluminescence.

2.5. Exosome-RNA extraction

Total exosome-RNA was isolated from exosomes using the exoRNeasy Midi Kit (Qiagen, Germany) following the kit's protocols.

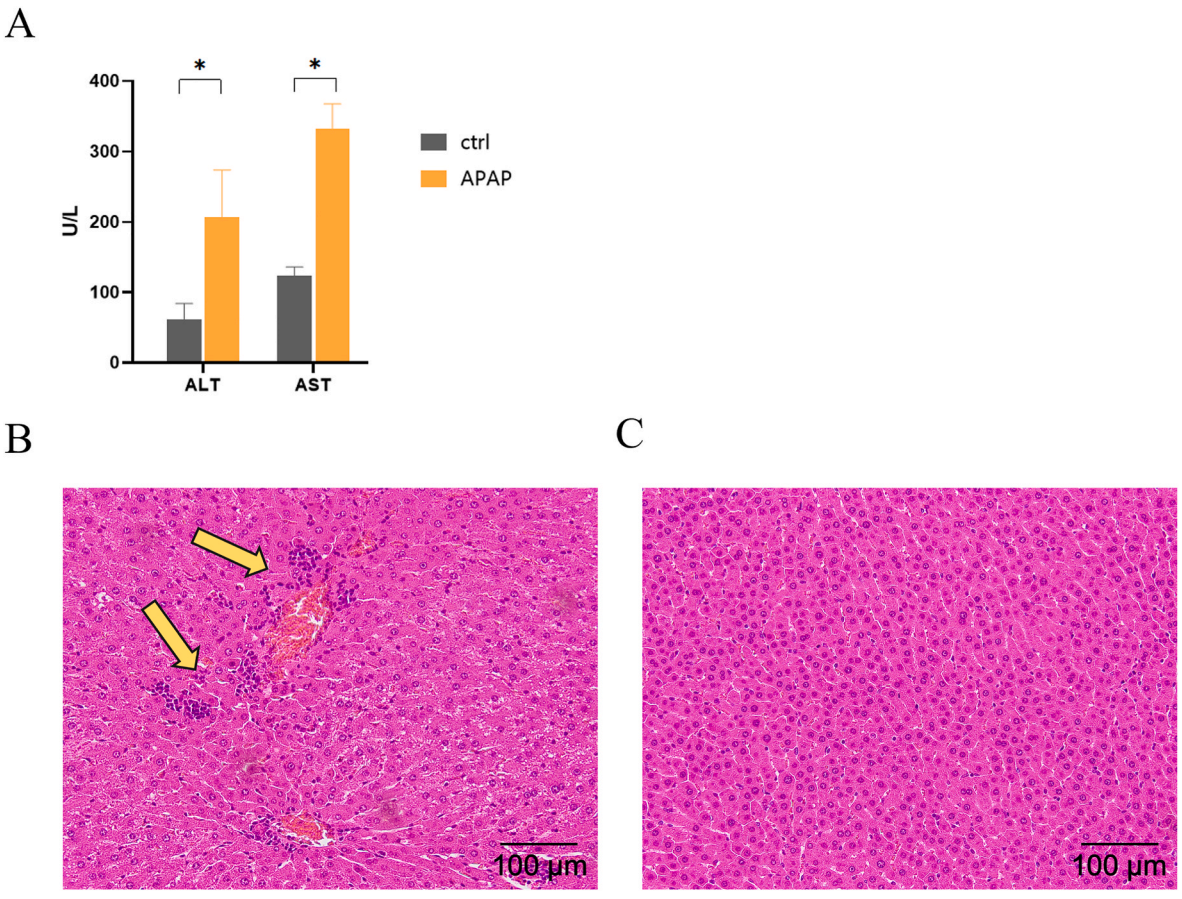

Fig. 1. (1A) The serum levels of ALT and AST in 2 groups. (1B & 1C) The histological images of APAP-induced hepatocellular injury group and control group (24 h).

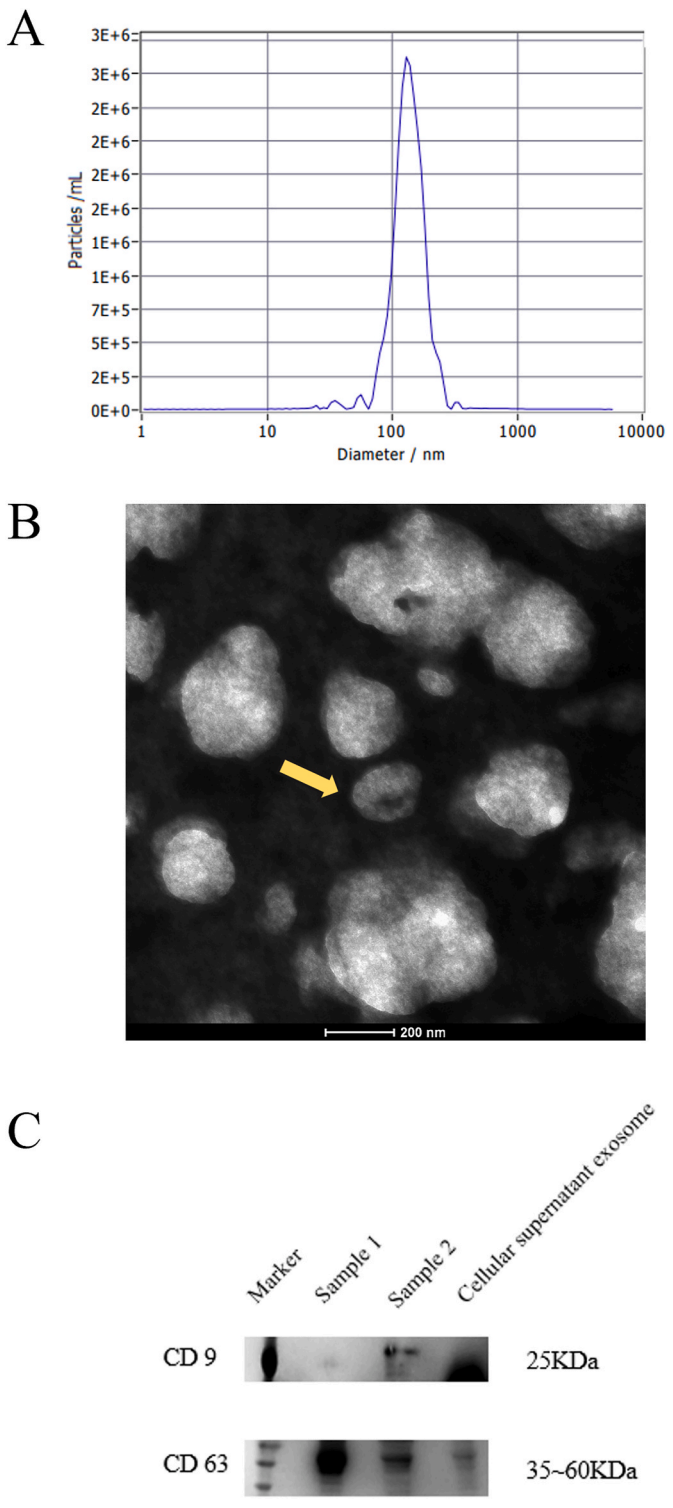

Fig. 2. Characterization of isolated exosomes. (2A) NTA of exosomes. (2B) TEM images of isolated plasma exosome. (2C) WB analysis of CD9 and CD63 expression levels in isolated plasma-derived exosomes.

2.6. RNA sequencing and functional enrichment analysis

Following the isolation of total exosome-RNA, libraries were established using an ultra-high-sensitivity microsample chain specificity kit. The constructed libraries underwent concentration measurement using a Qubit® 2.0 Fluorometer and library size analysis using Agilent2100. Qualified libraries were prepared for Illumina sequencing using a PE150 sequencing strategy. For lncRNA prediction and quantification, Stringtie (v1.3.0) was utilized along with the NONCODE database (v2016; http://www.noncode.org/), in addition to known LncRNAs from the Ensembl database. Identified LncRNAs were categorized into 3 types: MSTRG (novel LncRNAs), NON (previously known LncRNAs), and ENS (LncRNAs annotated in the Ensembl database).

Gene Ontology (GO) analysis was conducted to identify enriched terms in cellular components, molecular functions, and biological processes. Pathway analysis of differentially expressed genes obtained from RNA-seq data was carried out using the KEGG database, with significant pathways determined using Fisher's exact test.

To construct lncRNA-miRNA-mRNA regulatory axes, validated LncRNAs were initially selected. Target RNAs of miRNAs were predicted based on miRNA response element sequences using the miRNA target prediction software, miRanda. Default settings were used, and intersected target RNAs were retained. Subsequently, the regulatory network was constructed using Cytoscape software (v3.10.1).

2.7. Quantitative real-time PCR

Eight differentially expressed LncRNAs were validated through qRT–PCR. Primer pairs were formulated using the back-spliced sequences as a reference. Firstly, cDNA synthesis was conducted using the ReverTra Ace™ qPCR RT Kit (TOYOBO, Japan) in a 20-μl reaction volume. Subsequently, real-time PCR was conducted on an Applied Biosystems 7500 Real-time PCR Analyzer (Applied Biosystems, USA) using Power SYBR Green PCR Master Mix (Applied Biosystems, USA). The reaction conditions were as follows: 50 °C for 2 min, followed by 95 °C for 10 min, and then 40 cycles of 15s at 95 °C and 60 s at 60 °C. The average Ct value was utilized to determine the relative expression of LncRNA using the comparative $2^{-\triangle\triangle Ct}$ approach. GAPDH served as a reference gene. Primer pairs were designed and synthesized by Thermo Fisher Scientific (Guangzhou, China). The primer sequences employed are listed in Table 1.

2.8. Statistical analysis

The data are presented as mean ± standard deviation (SD) and were subjected to group comparisons. Statistical tests were performed using GraphPad Prism 9 (GraphPad, USA) and SPSS 22.0 (IBM, USA). Student's t-test was utilized to evaluate differences between two groups if the data distribution adhered to a normal distribution with equal variance. A significance level was set at $P < 0.05$.

3. Results

3.1. Establishment of APAP-induced hepatocellular injury

Twenty Sprague-Dawley rats, evenly divided between male and female, received APAP at a dosage of 1250 mg/kg through intragastric administration (n = 10). The control rats (n = 10) were administered 0.5 % CMC-Na solvent. After 24 h, all samples were collected. Serum ALT and AST levels were significantly elevated in the experimental group compared to the control group. Necrosis with an inflammatory reaction was observed, indicated by the yellow arrow. Both histological and biochemical analyses confirmed the successful induction of hepatocellular injury by APAP (Fig. 1).

3.2. Exosome characterization

The effective isolation of exosomes is crucial for examining the characteristics of exosomal LncRNA expression. To achieve this, we employed NTA to assess the size and concentration of exosomes (Fig. 2A). Our findings, illustrated in Fig. 2, revealed that plasma exosomes ranged in diameter from 50 nm to 200 nm, with a concentration of 2.5×10^{10} particles/mL (the result of a 1000-fold dilution). The size

Table 2
Part of DE-LncRNAs.

LncRNA ID	log_2FC	P(values)	Regulation	Locus
NONRATT018001.2	7.31949	0.00011	UP	3:8770347–8770762
NONRATT004188.2	2.643694568	0.019558793	UP	10:31237556–31240582
NONRATT008284.2	2.712156585	0.043725475	UP	13:60529819–60538965
MSTRG.62141.8	−8.524402878	0.00124	down	5:47406065–47410187
NONRATT012135.2	−7.081812999	0.001163	down	16:81636835–81637726
ENSRNOT00000090877	−5.51646	0.012277	down	13:101999190–102018787

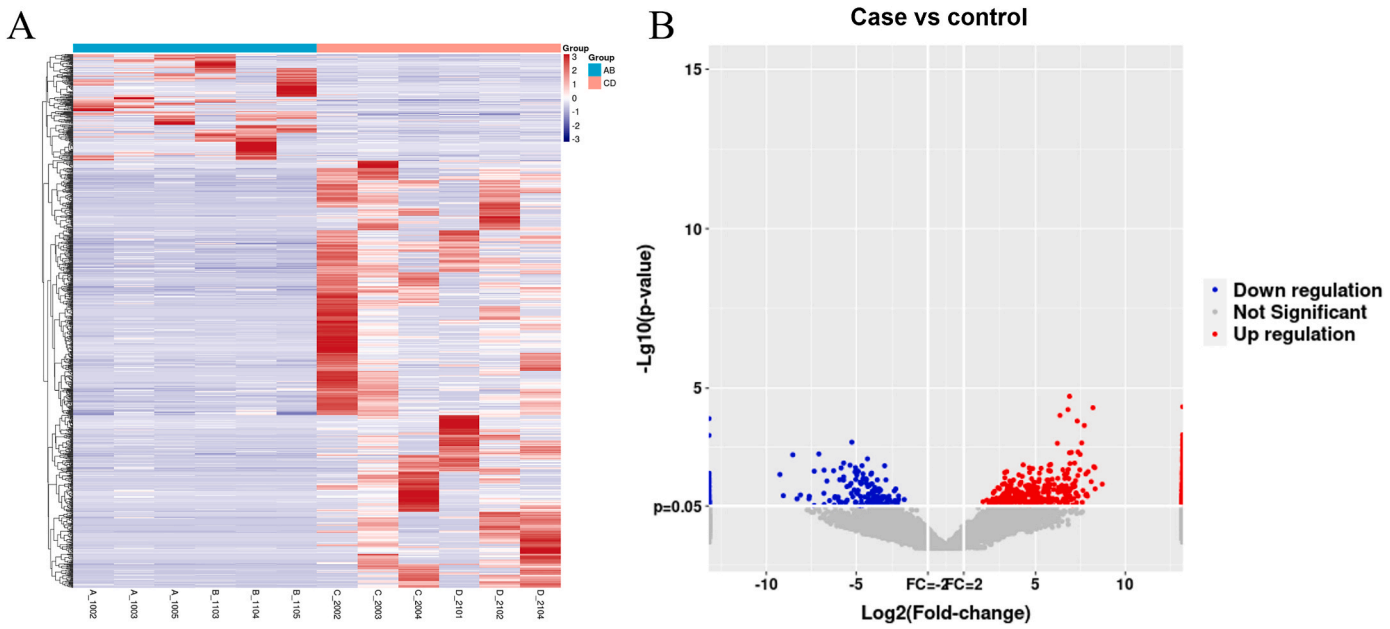

Fig. 3. The expression patterns of LncRNAs in rats' plasma exosome: (3A) Heatmap of LncRNAs revealing hierarchical clustering of altered LncRNAs; red and blue denote up- and down-regulated genes, respectively; (3B) Volcano plot displaying up- and down-regulated LncRNAs; Red, blue and gray represent up-regulated, down-regulated, and non-significantly expressed genes, respectively.

distribution exhibited a peak at 135.4 nm, indicating the modal size of exosomes.

TEM examination (Fig. 2B) allowed us to identify exosomes in the plasma sample by their characteristic cup-shaped morphology and size, as indicated by the yellow arrow.

Furthermore, WB analysis (Fig. 2C) targeting exosome tetraspanins CD9 and CD63 was performed on exosomes isolated from plasma samples using the Qiagen exoRNeasy Midi Kit. CD9 and CD63 were detected in two samples, confirming the presence of exosomes.

The results from NTA, TEM, and WB analysis all confirmed that the material extracted from rat plasma using the exoRNeasy Midi Kit (Qiagen, Germany) was indeed exosomes. Exosomes typically range from 30 to 150 nm in diameter, with a peak size of 135.4 nm observed in the NTA analysis. In TEM images, the characteristic cup-shaped morphology and size were indicative of exosomes. Additionally, WB analysis revealed the presence of exosome tetraspanins CD9 and CD63 in the samples.

3.3. Differential expression and cluster analysis of LncRNAs

A total of 458 exosomal DE-LncRNAs were identified, according to $log_2FC > |\pm 2.0|$ and $p < 0.05$, comprising 321 and 137 upregulated and 137 downregulated LncRNAs, respectively. In addition, employing a stricter threshold of $log_2FC > |\pm 4.0|$, there were 231 and 90 upregulated and downregulated LncRNAs, respectively. Comparatively, under more stringent conditions of log_2 fold change $> |\pm 8.0|$, 6 LncRNAs were upregulated and 5 were downregulated, when compared to the control group. Part of the list of exosomal DE-LncRNAs is presented in Table 2. These findings suggest a close association between exosomal DE-LncRNAs and the development and progression of APAP-induced hepatocellular injury. A volcano plot and a clustered heatmap were used to show the expression patterns of exosomal DE-LncRNAs (Fig. 3).

3.4. Comprehensive functional characterization of exosomal DE-LncRNAs

To explore the potential functional implications of observed alterations in LncRNA levels between the control and injury groups, we conducted a GO term enrichment analysis. We demonstrated the remarkably enriched GO terms of exosomal DE-LncRNAs (Fig. 4A) pertaining to molecular functions, cellular components, and biological processes. Furthermore, to ascertain whether specific pathways were altered in APAP-induced hepatocellular injury, we performed KEGG enrichment analysis on the target genes of exosomal DE-LncRNAs (Fig. 4C). The pathways exhibiting more pronounced differences included Rap1 [20], PI3K-Akt [20], and cAMP [21], all commonly associated with liver injury, aligning with findings from previous studies [20,21]. This indicates that the selected exosomal DE-LncRNAs in this study might interact with key genes within these pathways. Consequently, their expression levels could potentially fluctuate in response to changes in pathway activation during injury.

3.5. Quantitative real-time PCR validation for RNA sequencing

In order to verify exosomal DE-LncRNAs, we replicated APAP-induced hepatocellular injury using procedures identical to those in the previous experiment. However, in this study, we focused solely on

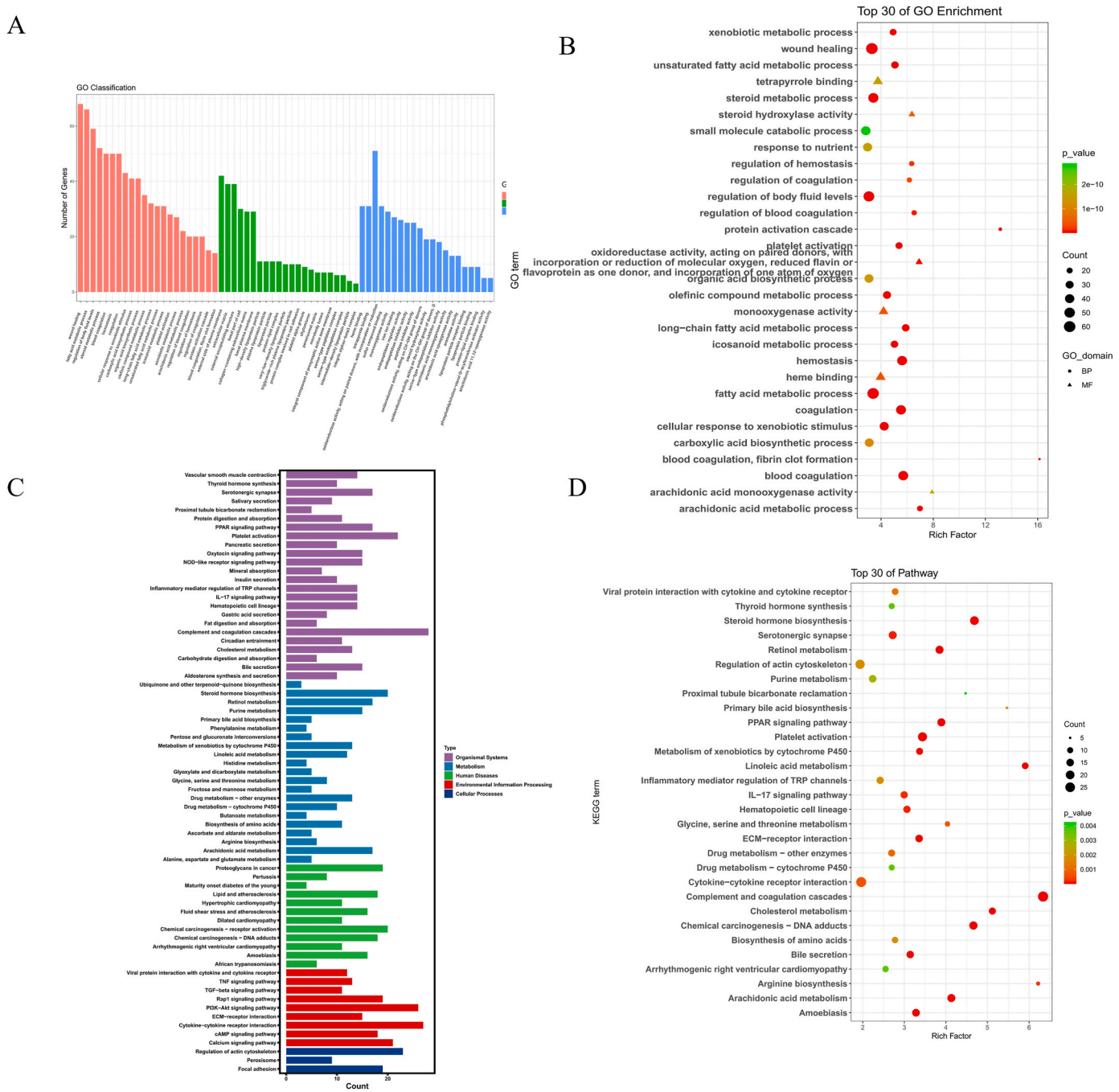

Fig. 4. GO and KEGG analyses of exosomal differentially expressed LncRNAs target genes in rats' plasma exosome from the case and control groups: (4A) GO categories of exosomal DE-LncRNAs target genes from the patient and control groups. (4B) Top 30 of GO categories. (4C) KEGG analysis of exosomal DE-LncRNAs target genes from the patient and control groups. (4D) Top 30 of KEGG analysis.

verifying the upregulated LncRNAs. Eight LncRNAs were selected for validation: NONRATT018001.2, MSTRG.46987.1, MSTRG.73954.4, NONRATT013926.2, NONRATT004188.2, NONRATT008284.2, NONRATT023507.2, and NONRATT029616.2.

The verification results are shown in Fig. 5. For male Sprague-Dawley rats, compared to the control group, the expression levels of NONRATT018001.2 ($p < 0.05$), MSTRG.73954.4 ($p < 0.05$), and NONRATT004188.2 ($p > 0.05$) exhibited a more than 2-fold increase. However, the expression levels of the remaining five LncRNAs were less than 2-fold, rendering them ineligible for further consideration. For female Sprague-Dawley rats, the expression levels of all eight LncRNAs were less than 2-fold, and unfortunately, the p-values were greater than 0.05. To a certain extent, the validation results were in agreement with the expression profiles of LncRNAs acquired through RNA-seq. Given that male Sprague-Dawley rats demonstrated more promising results compared to females, we selected NONRATT018001.2 and MSTRG.73954.4 for further experiments and designed subsequent experiments specifically utilizing male Sprague-Dawley rats.

3.6. Changes in histology and biochemical analysis, and sensitivity comparison of two LncRNAs

3.6.1. Hepatocellular injury model

Over time (at 1.5, 3, 6, 12, and 24 h post-administration), the

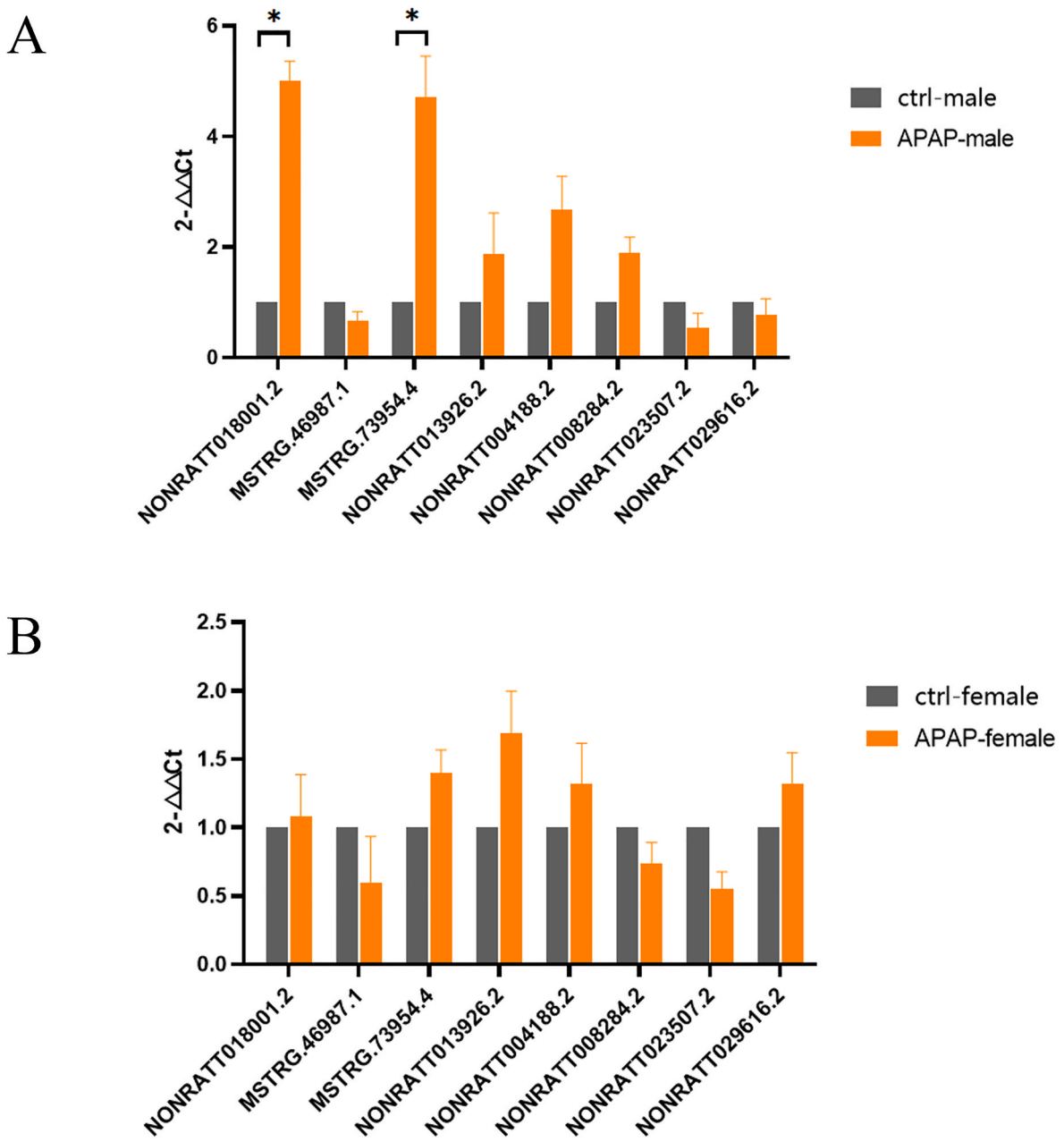

Fig. 5. The expression of exosomal LncRNAs in APAP-induced hepatocellular injury model, validated by qPCR. Six specimens (3 males and 3 females) were selected from the patient and control groups (Mean ± SD). *p < 0.05.

expression levels of the two candidate LncRNAs gradually increased (Fig. 6D). No significant differences in ALT and AST levels were observed at 1.5, 3, 6, and 12 h post-administration (Fig. 6C), while HE staining revealed no specific lesion sites. Necrosis accompanied by inflammatory reactions was evident (Fig. 6A), indicated by yellow arrows. Notably, changes in our candidate LncRNAs preceded alterations in serum biomarkers and histological findings.

3.6.2. *Intrahepatic cholestasis model*

Similarly, the expression levels of the two candidate LncRNAs increased at 1.5, 3, 6, 12, and 24 h post-administration (Fig. 7D). No significant differences in ALT and AST levels were observed at the specified time points (Fig. 7C), and HE staining indicated no focal lesions. However, intrahepatic bile duct hyperplasia was observed (Fig. 7A), highlighted by yellow arrows. Once again, changes in the candidate LncRNAs occurred earlier than alterations in serum biomarkers and histology.

3.6.3. *Fatty liver model*

Following 3, 7, 14, 21, and 28 days of feeding, the expression levels of the two candidate LncRNAs increased (Fig. 8D). No significant differences in ALT and AST levels were observed up to 21 days (Fig. 8C). However, at day 7, the expression levels of both candidate LncRNAs exceeded 2-fold and 4-fold, respectively, and HE staining revealed minor steatosis (Fig. 8A), marked by yellow arrows. Notably, changes in the candidate LncRNAs preceded alterations in serum biomarkers.

3.6.4. *Hepatic fibrosis model*

At 14, 28, 42, 49, and 56 days post-administration, the expression levels of both candidate LncRNAs increased (Fig. 9D). Significant differences in ALT and AST levels were observed at all time points (Fig. 9C), and HE staining revealed hepatocellular necrosis and fibrosis at day 49

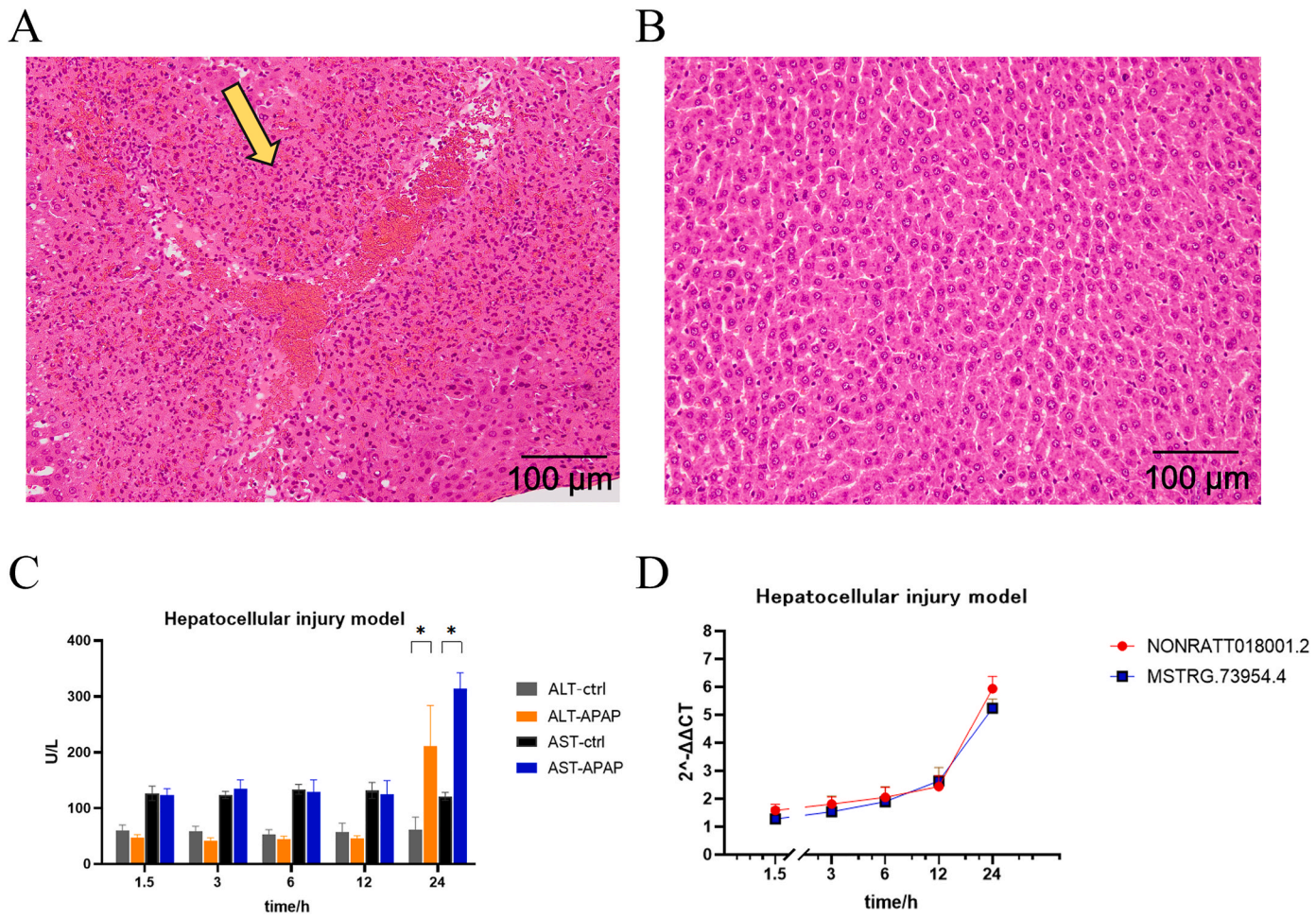

Fig. 6. (6A & 6B) The histology images of APAP-induced hepatocellular injury group and control group (24 h) (6C) The serum levels of ALT and AST in thr two groups. (6D) The expression of 2 candidate LncRNAs in APAP-induced hepatocellular injury model, validated by qPCR. *: $p < 0.05$.

(Fig. 9A), indicated by yellow arrows. Interestingly, changes in the candidate LncRNAs preceded alterations in serum biomarkers and histology by day 28.

3.6.5. *Myocardial injury model*

As AST is recognized as a serum biomarker for liver injury, its elevation may also occur during myocardial injury. Hence, we induced IH-related myocardial injury to investigate whether candidate LncRNAs could discern between liver and myocardial injury. Serum levels of high-sensitivity troponin I (hsTnI) were significantly higher in myocardial injury group than in control group ($p < 0.01$, Fig. 10A). CK and AST levels also exhibited obvious differences between the patient and control groups ($p < 0.05$, Fig. 10B). Notably, myocardial degeneration and necrosis were evident (Fig. 10C), indicated by yellow arrows. However, candidate LncRNAs showed no significant differences between the case and control groups (Fig. 10E).

In summary, across the four liver injury models, both exosomal NONRATT018001.2 and exosomal MSTRG.73954.4 exhibited earlier elevation compared to ALT and AST, albeit to varying degrees. Most blood collection points did not indicate specific lesion sites, while the two exosomal LncRNAs showed significant differences, suggesting they possess greater sensitivity than ALT and AST. In the IH-related myocardial injury model, the two exosomal LncRNAs did not display significant differences between the case and control groups, indicating their potential to distinguish between different types of organ injury when AST fails to do so. Therefore, exosomal LncRNAs, specifically NONRATT018001.2 and MSTRG.73954.4, have already demonstrated potential as biomarkers.

3.7. *LncRNA-miRNA-mRNA co-expression network*

Pearson's correlation coefficients were computed to assess the relationship between the expression levels of each LncRNA-miRNA-mRNA triplet across samples from both groups ($p < 0.05$). Subsequently, we constructed a co-expression network of LncRNA-miRNA-mRNA interactions using Cytoscape (Fig. 11). The network is comprised exclusively of upregulated exosomal DE-LncRNAs. Additionally, based on prior validation, we also generated a co-expression network specifically for NONRATT018001.2 and MSTRG.73954.4.

4. Discussion

Numerous studies have explored the roles of exosomes in various diseases, and the significance of exosomes in DILI has garnered increasing attention. DILI refers to the unforeseen harm inflicted on hepatocytes and other non-parenchymal liver cells by drugs or their metabolites [12]. It stands as the leading cause of hepatic injury, with APAP responsible for nearly half of ALF cases in the United States [13]. Given the liver's crucial role in metabolizing and concentrating xenobiotics, it serves as the primary site for drug-induced injury. Severe DILI represents a critical clinical manifestation and a primary reason for ALF, often necessitating liver transplantation.

In recent years, liquid biopsy has emerged as a promising diagnostic and prognostic tool. Liquid biopsy involves the analysis of liquid

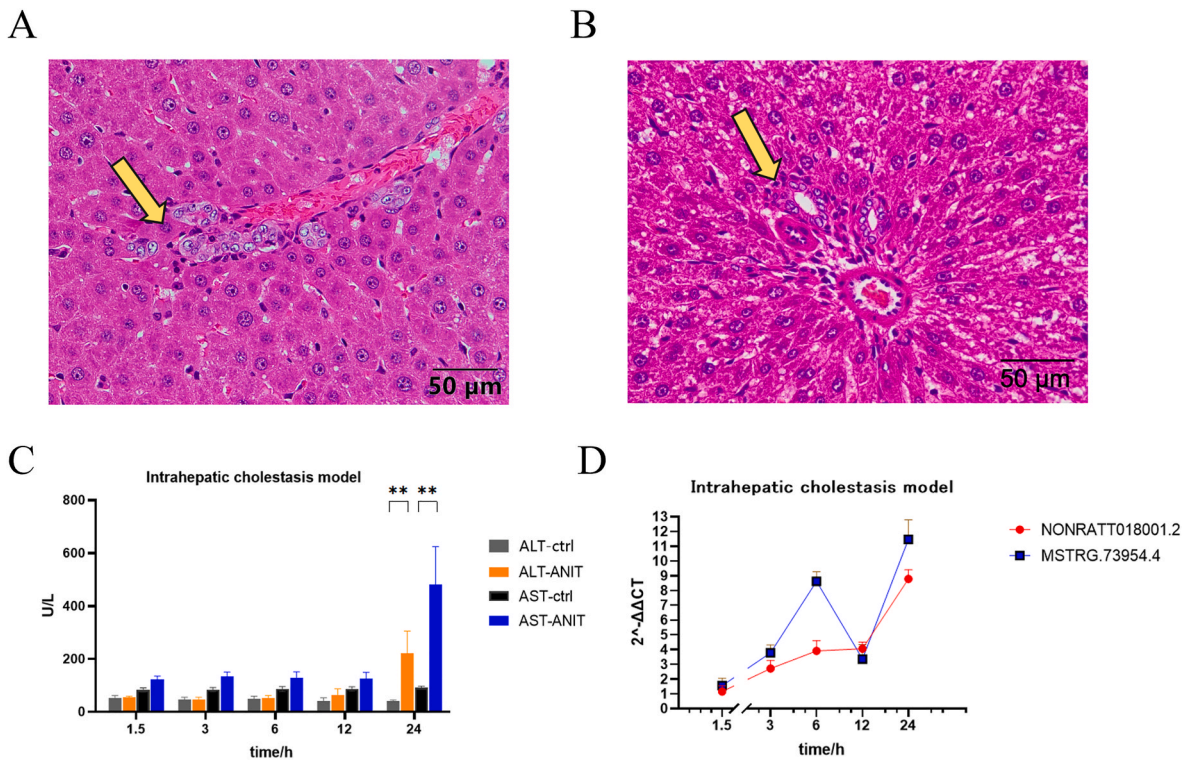

Fig. 7. (7A & 7B) The histology images of intrahepatic cholestasis model group and control group (24 h). (7C) The serum levels of ALT and AST in the two groups. (7D) The expression of 2 candidate LncRNAs in intrahepatic cholestasis model, verified by qPCR. **p < 0.01.

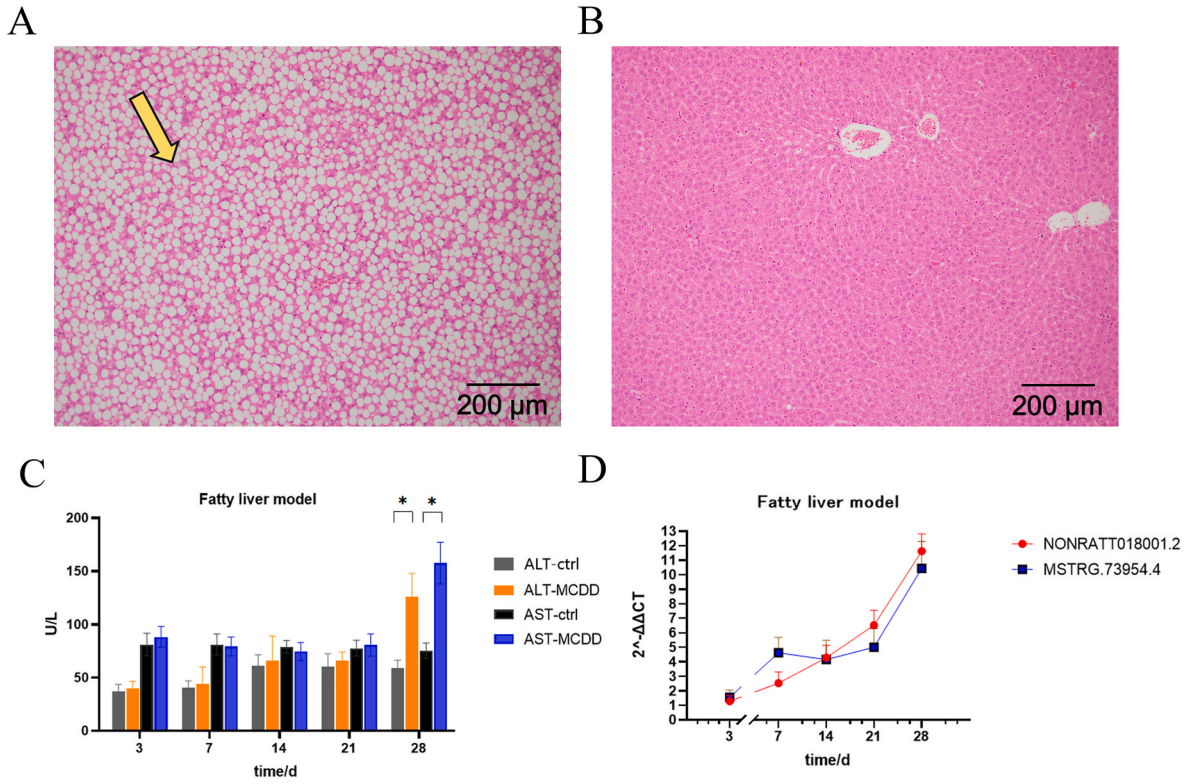

Fig. 8. (8A & 8B) The histology images of fatty liver group and control group (28 h) (8C) The serum levels of ALT and AST in the two groups. (8D) The expression of 2 candidate LncRNAs in fatty liver model, verified by qPCR. *p < 0.05.

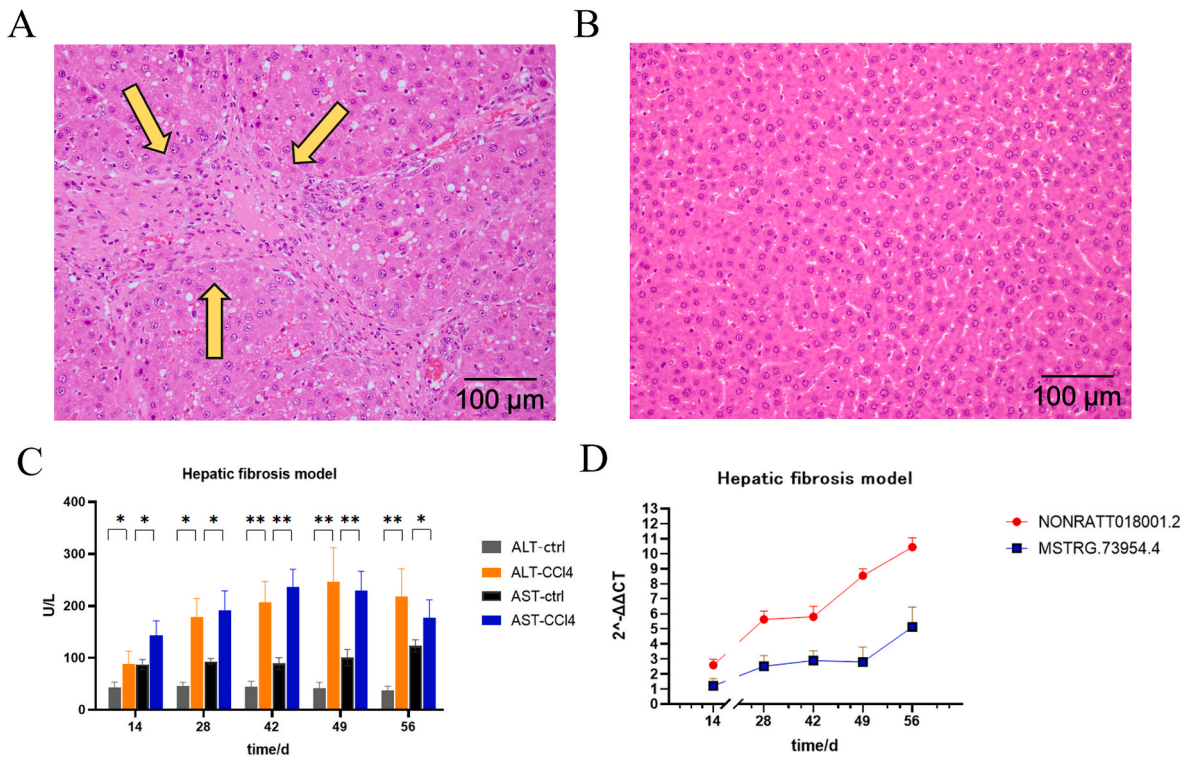

Fig. 9. (9A & 9B) The histology images of hepatic fibrosis group and control group (56 days) (9C) The serum levels of ALT and AST in the two groups. (9D) The expression of 2 candidate LncRNAs in hepatic fibrosis model, verified by qPCR. *p < 0.05, **p < 0.01.

biological samples such as blood, ascitic fluid, or urine to assess valuable biomarkers. Exosomes, as carriers of molecular cargo reflective of their cell of origin, present novel biomarkers suitable for evaluation in liquid biopsies. Plasma, due to its easy accessibility and the potential for sequential sampling at different time points, is among the most frequently utilized biological fluids for liquid biopsy. With the aid of cutting-edge genomic and proteomic technologies, plasma can furnish robust biological data for diverse applications. Liquid biopsy technologies have witnessed significant advancements over the past decade, notably with the advent of next-generation sequencing [14].

While ALT and AST enzymes serve as the conventional gold standard biomarkers for DILI, they lack liver specificity. Consequently, there is a pressing need for more specific and sensitive biomarkers for DILI diagnosis in both preclinical and clinical settings. Several advantages accompany the utilization of exosome-based DILI biomarkers. Firstly, circulating exosomes exhibit greater specificity in identifying DILI compared to currently employed biomarkers, as they reflect the status of the originating cells [15]. Secondly, exosomes can shield their nucleic acid and protein cargo from decomposition, extending the window for DILI detection [16,17]. Thirdly, the quantity of exosomes and their specific components, indicative of tissue cell metabolism, offer deeper insights into DILI mechanisms and provide supplementary evidence to identify the responsible medication [18]. Lastly, protein or nucleic acid biomarkers, abundant in exosomes but constituting only a minute fraction of plasma and serum, can be exclusively detected within isolated exosomes.

In this study, we used RNA sequencing to screen out exosomal DE-LncRNAs. Prior to RNA sequencing, we verified the successful induction of APAP-induced liver injury through histological and biochemical analyses. TEM, NTA and WB analysis were employed for exosome characterization, with all results confirming the presence of exosomes. Functional enrichment analysis and co-expression network were conducted to elucidate the mechanisms underlying the association between exosomal DE-LncRNAs and APAP-induced liver injury. Additionally, we established four other liver injury models to investigate whether NONRATT018001.2 and MSTRG.73954.4 exhibited changes earlier than conventional biomarkers (ALT and AST) and histological alterations. Each model involved five time points. In the hepatocellular injury and intrahepatic cholestasis models, both NONRATT018001.2 and MSTRG.73954.4 demonstrated earlier increases compared to serum biomarkers, while histological changes were not observed until the final time point. In the fatty liver model, increases in NONRATT018001.2 and MSTRG.73954.4 preceded those of ALT and AST by 21 days. Notably, on the 7th day, despite minor steatosis observed in liver tissue, the expression levels of both candidate LncRNAs exceeded 2- and 4-fold, respectively. In the hepatic fibrosis model, both NONRATT018001.2 and MSTRG.73954.4 increased at all time points, with NONRATT018001.2 surpassing 8-fold on the 49th day, coinciding with the onset of hepatocellular necrosis and fibrosis. However, in the myocardial injury model, no obvious differences were observed between the patient and control groups for either NONRATT018001.2 or MSTRG.73954.4. In summary, NONRATT018001.2 and MSTRG.73954.4 exhibited the potential to distinguish between different organ injuries caused by drugs and predict various types of liver injury at an early stage, suggesting their utility as biomarkers. Future steps in our experiment may involve siRNA interference or gene knockout techniques to further elucidate the mechanisms underlying NONRATT018001.2 and MSTRG.73954.4.

Although exosomes hold promise as novel biomarkers for DILI, it is essential to address some limitations. Foremost among these is the absence of universally accepted standardization in exosome isolation techniques. Despite significant advancements in this field, each technique or method possesses its own set of benefits and drawbacks, as variations in the purity, type, and quantity of exosomes can obviously impact isolation outcomes. Moreover, factors such as sample collection conditions, storage protocols, and protein/RNA isolation methods can influence subsequent protein and RNA patterns [19]. Therefore, comprehensive efforts are warranted to develop standardized protocols for exosome isolation, preservation, and purification, applicable in both preclinical and clinical settings.

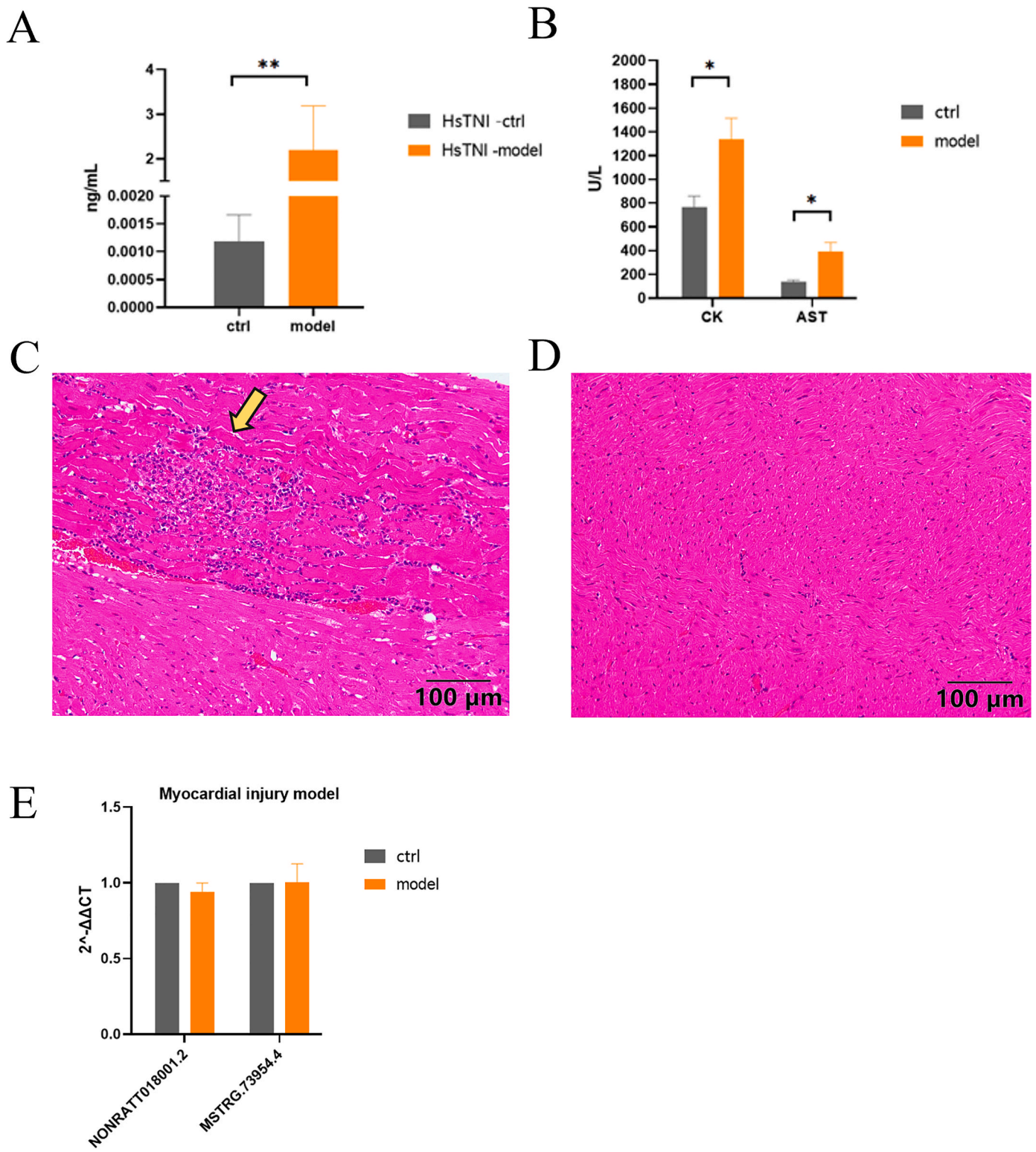

Fig. 10. (10A & 10B) The serum levels of hsTnI, CK and AST in the two groups; (10C & 10D) The histology images of myocardial injury group and control group (4 h). (10E) The expression of 2 candidate LncRNAs in myocardial injury model, validated by qPCR. *p < 0.05, **p < 0.01.

5. Conclusion

In conclusion, we identified two specific exosomal LncRNAs, NONRATT018001.2 and MSTRG.73954.4, as potential biomarkers for predicting various types of liver injuries at an early stage. These LncRNAs demonstrated distinct patterns of expression in response to different liver injury models, showing earlier increases compared to conventional biomarkers such as ALT and AST. Moreover, their expression levels correlated with histological alterations characteristic of liver injury, further validating their potential as biomarkers. These findings may provide valuable insights into the development of novel diagnostic and prognostic tools for liver diseases, particularly DILI. Nevertheless, further studies are warranted to fully elucidate the clinical utility and underlying mechanisms of these biomarkers.

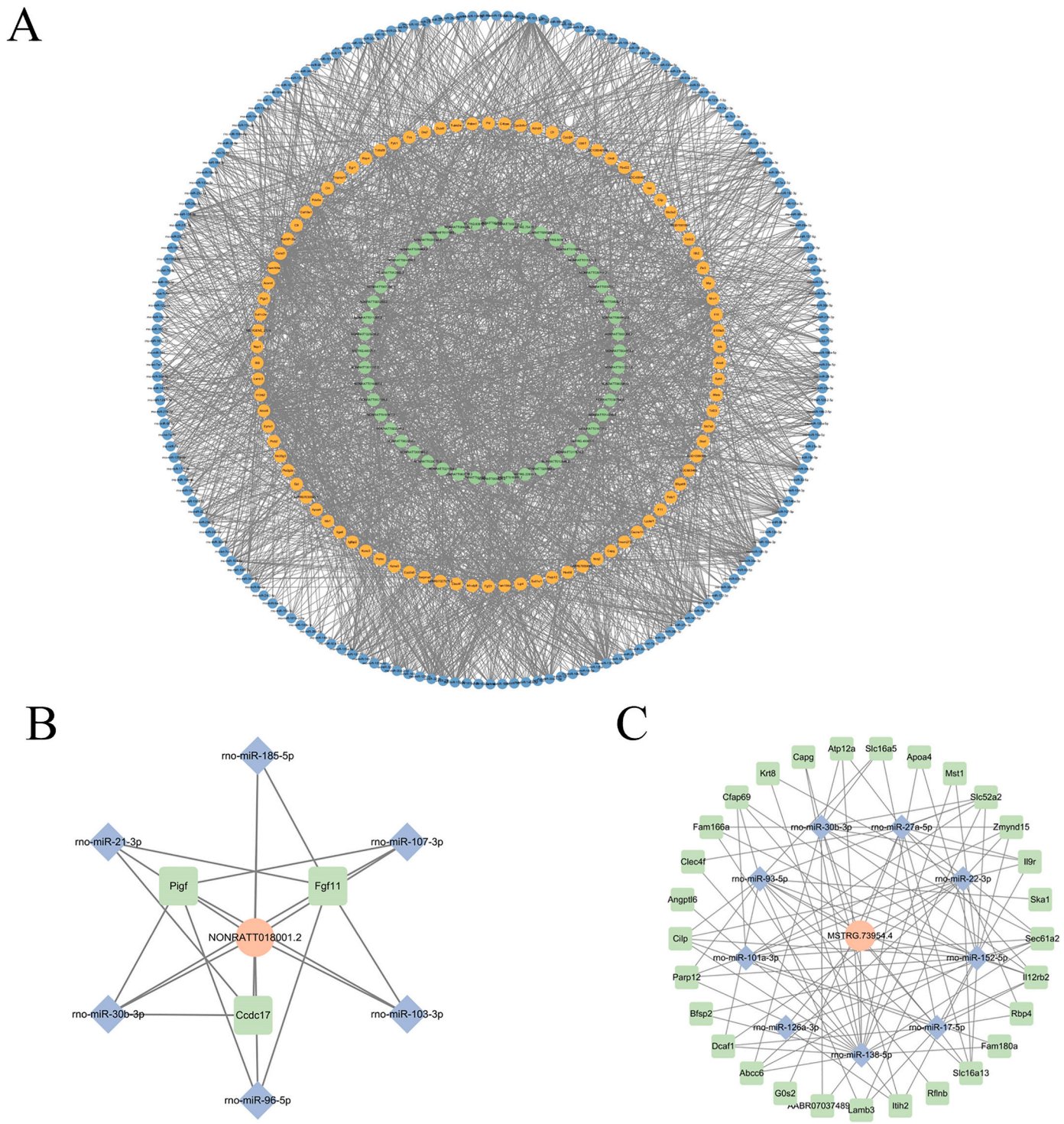

Fig. 11. LncRNA-miRNA-mRNA co-expression network: The red, blue and green nodes denote LncRNAs, miRNAs and mRNAs, respectively.

Funding

This study received no funding.

Ethics approval and consent to participate

Not applicable.

CRediT authorship contribution statement

Zixuan Yang: Writing – original draft, Validation, Software, Methodology, Investigation, Formal analysis, Data curation. **Lei Shi:** Writing – original draft, Validation, Software, Methodology, Investigation, Formal analysis, Data curation. **Minhui Zheng:** Writing – original draft, Validation, Investigation, Data curation. **Minbo Hou:** Writing – original draft, Software, Methodology. **Mengdi Zhou:** Software, Formal analysis, Data curation. **Naying Su:** Formal analysis, Data curation. **Hui Lang:** Software, Data curation. **Liyuan Zhao:** Investigation, Data curation.

Mengyun Gu: Investigation. **Naping Tang:** Writing – review & editing, Supervision, Project administration, Methodology, Conceptualization. **Yan Chang:** Writing – review & editing, Supervision, Project administration, Methodology, Conceptualization.

Acknowledgements

The authors gratefully acknowledge the helpful assistance of all personnel in completing the scientific work.

References

[1] R.J. Andrade, N. Chalasani, E.S. Bjornsson, A. Suzuki, G.A. Kullak-Ublick, P. B. Watkins, et al., Drug-induced liver injury, Nat. Rev. Dis. Prim. 5 (2019) 58.
[2] N. Kaplowitz, Idiosyncratic drug hepatotoxicity, Nat. Rev. Drug Discov. 4 (2005) 489–499.
[3] M.I. Lucena, N. Kaplowitz, H. Hallal, A. Castiella, M. Garcia-Bengoechea, P. Otazua, et al., Recurrent drug-induced liver injury (DILI) with different drugs in the Spanish Registry: the dilemma of the relationship to autoimmune hepatitis, J. Hepatol. 55 (2011) 820–827.
[4] P.N. Newsome, N.C. Henderson, L.J. Nelson, C. Dabos, C. Filippi, C. Bellamy, et al., Development of an invasively monitored porcine model of acetaminophen-induced acute liver failure, BMC Gastroenterol. 10 (2010) 34.
[5] E.S. Bjornsson, O.M. Bergmann, H.K. Bjornsson, R.B. Kvaran, S. Olafsson, Incidence, presentation, and outcomes in patients with drug-induced liver injury in the general population of Iceland, Gastroenterology 144 (2013) 1419–1425, 1425 e1411-1413; quiz e1419-1420.
[6] A. Reuben, H. Tillman, R.J. Fontana, T. Davern, B. McGuire, R.T. Stravitz, et al., Outcomes in adults with acute liver failure between 1998 and 2013: an observational cohort study, Ann. Intern. Med. 164 (2016) 724–732.
[7] Petra Thulin, Robert J. Hornby, Mariona Auli, et al., A longitudinal assessment of miR-122 and GLDH as biomarkers of drug-induced liver injury in the rat, Biomarkers 22 (5) (2017 Jul) 461–469.
[8] M.R. McGill, C.D. Williams, Y. Xie, A. Ramachandran, H. Jaeschke, Acetaminophen-induced liver injury in rats and mice: comparison of protein adducts, mitochondrial dysfunction, and oxidative stress in the mechanism of toxicity, Toxicol. Appl. Pharmacol. 264 (3) (2012) 387–394.
[9] C. Lasser, M. Eldh, J. Lotvall, Isolation and characterization of RNA-containing exosomes, J. Vis. Exp. 9 (59) (2012) e3037.
[10] C.K. Das, B.C. Jena, I. Banerjee, et al., Exosome as a novel shuttle for delivery of therapeutics across biological barriers, Mol. Pharm. 16 (1) (2019) 24–40.
[11] S.-P. Li, Z.-X. Lin, X.-Y. Jiang, et al., Exosomal cargo-loading and synthetic exosome-mimics as potential therapeutic tools, Acta Pharmacol. Sin. 39 (4) (2018) 542–551.
[12] R.J. Andrade, N. Chalasani, E.S. Bjornsson, A. Suzuki, G.A. Kullak-Ublick, P. B. Watkins, H. Devarbhavi, M. Merz, M.I. Lucena, N. Kaplowitz, G.P. Aithal, Druginduced liver injury, Nat. Rev. Dis. Prim. 5 (1) (2019) 58.
[13] G. Ostapowicz, R.J. Fontana, F.V. Schiodt, A. Larson, T.J. Davern, S.H. Han, T. M. McCashland, A.O. Shakil, J.E. Hay, L. Hynan, J.S. Crippin, A.T. Blei, G. Samuel, J. Reisch, W.M. Lee, U.S.A. Group, Results of a prospective study of acute liver failure at 17 tertiary care centers in the United States, Ann. Intern. Med. 137 (12) (2002) 947–954.
[14] I. Manea, R. Iacob, S. Iacob, R. Cerban, S. Dima, G. Oniscu, I. Popescu, L. Gheorghe, Liquid biopsy for early detection of hepatocellular carcinoma, Front. Med. 10 (2023) 1218705.
[15] X. Yang, Z. Weng, D.L. Mendrick, Q. Shi, Circulating extracellular vesicles as a potential source of new biomarkers of drug-induced liver injury, Toxicol. Lett. 225 (2014) 401–406.
[16] G. Raposo, W. Stoorvogel, Extracellular vesicles: exosomes, microvesicles, and friends, J. Cell Biol. 200 (2013) 373–383.
[17] E. van der Pol, A.N. Boing, P. Harrison, A. Sturk, R. Nieuwland, Classification, functions, and clinical relevance of extracellular vesicles, Pharmacol. Rev. 64 (2012) 676–705.
[18] Lanlan Zhao, Yuezhi Wang, Yu Zhang, The potential diagnostic and therapeutic applications of exosomes in drug-induced liver injury, Toxicol. Lett. 337 (2021 Feb 1) 68–77.
[19] S.K. Channavajjhala, M. Rossato, F. Morandini, A. Castagna, F. Pizzolo, F. Bazzoni, O. Olivieri, Optimizing the purification and analysis of miRNAs from urinary exosomes, Clin. Chem. Lab. Med. 52 (2013) 1–10. CCLM/FESCC.
[20] Shujing Lv, Honghong Yu, Xinyue Liu, Xiaoyan Gao, The study on the mechanism of hugan tablets in treating drug-induced liver injury induced by atorvastatin, Front. Pharmacol. (12) (2021 Jun 28) 683707.
[21] Fabio Alejandro Aguilar Mora, Nshunge Musheshe, Asmaa Oun, et al., Elevated cAMP protects against diclofenac-induced toxicity in primary rat hepatocytes: a protective effect mediated by the exchange protein directly activated by cAMP/cAMP-Regulated guanine nucleotide exchange factors, Mol. Pharmacol. 99 (4) (2021 Apr) 294–307.